Paper 05348, Corrosion/2005
NACE International, Houston, 2005

CORROSION OF ALUMINIZED STEEL IN SCALE-FORMING WATERS

Leonardo J. Cáseres and Alberto A. Sagüés
Department of Civil and Environmental Engineering, University of South Florida
Tampa, FL 33620, U.S.A.

ABSTRACT

Type 2 aluminized steel has a layered aluminum/Al-Fe coating on a carbon steel substrate. It has been proposed that carbonate scales formed from natural waters are protective to this material but concern existed about stability of the passive layer under those conditions. The behavior of type 2 aluminized steel was studied for >3,000 h in waters of controlled varying scaling tendencies containing different amounts of Ca^{+2} and HCO_3^- ions at room temperature and a moderate (370 ppm) chloride content. Initial findings showed extremely low corrosion rates under high total alkalinity and calcium carbonate precipitating tendencies. Corrosion performance was good over the test period in a high total alkalinity, non-scale forming medium but electrochemical impedance measurements indicated some corrosion in progress. Exposure to the same chloride content but in the absence of alkalinity or precipitating hardness led to early pitting of the aluminized layer.

Keywords: aluminized steel, corrosion, electrochemical impedance, scaling tendency

INTRODUCTION

Type 2 aluminized steel (T2AS) is produced as a steel sheet hot dip coated on both sides with commercially pure aluminum, which provides corrosion protection through low corrosion rate of the aluminum when it is passive, and by galvanic protection of exposed underlying steel under more aggressive conditions [1]. T2AS is increasingly used for metallic drainage components in contact with natural waters. Corrosion is an important durability limitation factor in these components which are often designed for very long service life (e.g. 75 years) [2]. Mechanistic knowledge of corrosion processes is needed to better forecasting durability in critical highway applications. In particular, it has been proposed [3,4] that calcium carbonate scales formed from natural waters are protective to aluminized steel.

A common indicator or scaling tendency is the Langelier Saturation Index, LSI = pH-pH_s, where pH_s is the pH that would result in $CaCO_3$ precipitation [5]. LSI>0 implies a tendency

for $CaCO_3$ precipitation. However, the LSI does not consider the reserve of species in the solution responsible for a given pH. Based on extensive field data, Bednar [4] proposed that the corrosion performance of T2AS in aerated media may be better predicted by the combination of an index indicating carbonate scaling tendency (BI=Total Alkalinity (TA) plus Total Hardness (TH) minus Free CO_2 (FC)) and the conductivity σ of the solution in contact with the alloy. However, there is concern that the aluminum-rich layer in T2AS could be susceptible to depassivation if the carbonate scale promotes alkaline conditions. For example, Porter and Hadden [6] stated that corrosion in pure aluminum was most severe in harder natural waters. This concern is addressed in the present work, where initial experiments to examine the room temperature behavior of T2AS in synthetic waters of controlled varying scaling tendencies are reported. Three environments were used corresponding to a carbonate precipitating condition (P), a mildly alkaline but non-precipitating condition (NP), and a neutral control. The conditions were obtained by adjusting the Ca^{+2} and HCO_3^- ion contents.

EXPERIMENTAL PROCEDURE

The T2AS tested was manufactured per ASTM A929, from low carbon steel (Table 1) coils rolled to 16 gage (~1.59 mm thick) and hot-dipped in a bath of commercially pure aluminum. The microstructure (Figure 1) had a pearlite-free ferrite substrate with equiaxed grains. The aluminized layer included a partly columnar inner layer ~10 μm thick, of approximate intermetallic composition Fe_2Al_5 [7] as determined by scanning electron microscopy (SEM) with energy dispersive x-ray analysis (EDS), and an outer layer ~20 μm thick. The composition of the gray outer layer matrix and the small lighter features was predominantly aluminum with ~2.4 wt% Fe and 6-11 wt% Fe respectively. The light features resemble Fe-rich precipitates identified elsewhere [8].

Circular test specimens of 95 cm^2 exposed surface area were cut out from the as-received sheet stock, cleaned with ethanol and acetone, and stored in a desiccator before immersion. A 500 mL three-electrode test cell configuration was used (Figure 2) exposing horizontally one of the specimen faces. An activated titanium mesh 5 cm away from the specimen surface was used as a counter electrode, while a low impedance activated titanium reference electrode [9] (0.3 cm diameter and 5 cm long) was placed ~1.5 cm apart from the specimen surface and periodically calibrated against a saturated calomel reference electrode (SCE).

Table 2 shows the target composition of the synthetic solutions, all made from reagent chemicals and de-carbonated de-ionized water of resistivity>10^6 ohm-cm. Combinations of NaOH and NaCl (solution C), $NaHCO_3$, NaCl, and HCl (solution NP), $NaHCO_3$, NaCl, HCl and $Ca(OH)_2$ (solution P) were used. The test solutions were aerated for 30 sec at a rate of ~0.03 cm^3/sec twice a day using CO_2-free air (for solution C) and ambient air (for solutions NP and P) and isolated from the external air the rest of the time. Values of FC were calculated based on the alkalinity and pH of the water [5]:

$$FC = \frac{TA \cdot 10^{-pH}}{10^{-6.35}} \quad (1)$$

Synthetic solutions C and NP had LSI = -5.9 and -0.6, respectively, whereas the solution P had LSI = +1.5. Indeed, solution P precipitated $CaCO_3$ to yield a ~0.5 mm thick powdery layer on the specimen surface shortly after initiation of the test exposure. To examine possible effects of thick precipitate formation in solution P tests, an extra 10 gr $CaCO_3$ reagent grade powder was poured into the cell after 312 hours and again after 480 hours to form ~5 mm and ~9 mm thick layers, respectively.

The immersion tests were conducted in duplicate for up to nearly 3,100 hours at 22±2 ˚C. Solution pH and electrical conductivity, and OCP of each specimen were monitored periodically. Electrochemical Impedance Spectroscopy (EIS) measurements were obtained at the OCP with a Gamry™ PCI4-300 potentiostat in the frequency range from 300 kHz to 1 mHz using sinusoidal signals of 10 mV rms amplitude. At the end of the test, the specimens were removed, cleaned, and visually examined.

RESULTS

Figure 3 exemplifies the OCP evolution of multiple specimens in the test solutions. Initial OCP was ~-600 mV in C and NP, and ~-800 mV in P. No crevice corrosion developed in any of the specimens.

After a few hours of immersion the potential in solution C dropped abruptly to ~-950 mV and stable isolated pits became visible to the naked eye. Afterwards, the OCP slowly increased toward a terminal value of ~-850 mV and a uniform, poorly adherent grayish layer formed on the surface. SEM-EDS analysis of a dried portion fraction of that layer showed results consistent with the presence of aluminum hydroxide.

In solutions P and NP the terminal potentials were in the order of ~-780 mV and ~-930 mV respectively. However, the first addition of excess $CaCO_3$ to P caused short term negative and then positive OCP excursions by ~80 mV. The potential recovered slowly afterwards, little affected by the next $CaCO_3$ addition. Post exposure optical 25X examination revealed no pits on specimens exposed to solutions NP and P, very slight discoloration in NP and none in P. There were no visible precipitates in solution NP, while in solution P milky white deposits existed from the beginning. The P deposits and excess $CaCO_3$ washed off readily after exposure.

The initial pH of the test solutions closely approached the target values. In P the pH remained stable, increasing to only 7.8 after 3,000 hr. However, in NP the pH increased to 8.50 after 24 h and reached 8.80 at 3,000 hr. In C the pH was 7.7 after 3,000 h but reached a maximum of 8.85 at 310 h. Solution conductivity remained close to the target values. The Fe^{+2} content of the three solutions, measured by Atomic Absorption Spectroscopy after ~2,000 h, was <0.01 ppm.

The EIS results for NP (Figure 4) show an impedance diagram where the modulus at low frequencies (*lf*) initially increased with time, consistent with generally passive behavior and the absence of visual evidence of active corrosion. The *lf* modulus decreased later to values smaller than at the beginning, but even then its magnitude was large (>~200 $k\Omega$-cm^2). In P (Figure 5) the impedance magnitude was always large and showed an increasing *lf* modulus trend. However, upon each $CaCO_3$ addition the *lf* modulus showed a pronounced momentary

decrease and a slow later recovery. The diagrams were usually describable by two overlapping loops, both approaching ideal capacitive behavior.

In solution C (Figure 6) the *If* modulus was initially much smaller than in the NP and P solutions, and for a short initial period there was also a *If* inductive loop. After some exposure time the *If* modulus decreased even further (to ~ 68 $k\Omega$-cm^2) coinciding with the appearance of the grayish non adherent layer, but there was a long term recovery trend toward lager *If* moduli. The diagrams were usually describable by two overlapping loops, but unlike in the other solutions the high frequency loop deviated markedly from ideal capacitive behavior.

DISCUSSION

Direct evidence of corrosion performance

Visual examination of the specimen surfaces in the P and NP solutions indicated none or very little corrosion distress even after 3,000 hr of exposure, suggesting good corrosion performance in these environments that included high total alkalinity with and without carbonate precipitation. The addition of extra powdered $CaCO_3$ to solution P did not appear to have had harmful consequences despite momentary electrochemical disturbances. In contrast, pitting and discoloration was observed in solution C that had low alkalinity and no precipitating tendency. Corrosion during the time frame investigated appeared to be limited only to the aluminized layer.

EIS response and corrosion rate evaluation

The circuit chosen to simulate the impedance response of the P and NP systems is shown in Figure 7. R_S represents the ohmic solution resistance. The working assumption is made that the EIS response of the passive film, which occupies most of the specimen surface, is predominantly capacitive and represented by the constant phase angle element [(A)] CPE_F in the upper branch of the circuit. The film surface is taken to be the locus of a slow, nearly uniform anodic dissolution reaction, which is only mildly potential dependent so its admittance is neglected. The system is at the open potential and the matching cathodic reaction is assumed to occur primarily at film breaks, in particular at second phase precipitates such as those observed in the present system. Those singularities have been long recognized as important sites for cathodic reactions on aluminum [10]. The lower branch of the circuit represents the impedance of the integrated cathodic reaction at the singularities. To account for the observation of a low frequency loop in the impedance diagrams, the cathodic reaction is proposed to proceed in coupled steps of the type where surface coverage by an intermediate adsorbate alters the rate of the next step [11-14]. The resulting response is pseudocapacitive [(B)] (with capacitance given by element CPE_2) with a high-frequency limit resistance (or charge transfer resistance) R_{P1}, and a low frequency limit resistance (or polarization resistance) R_{P1} + R_{P2} [13]. Consequently, the capacitive term is across R_{P2} as shown.

[(A)] A Constant Phase Angle Element (CPE) has impedance $Z_{CPE} = 1/C^*(j\omega)^n$ where $\omega=2\pi f$, C* is a nominal capacitance such that if expressed in F it would be the value of an ideal capacitor having the same impedance modulus as the CPE at ω=1 Hz, and n is the dispersion coefficient.

[(B)] And also show pseudoinductive behavior, as it is sometimes observed in Aluminum [11,12], depending on the relative parameters of the coupled reactions.

This equivalent circuit yielded good best-fit simulations of the impedance response of both solutions, shown by the solid lines in Figures 4 and 5. Although CPEs were used in the circuit, the calculated parameters for both showed little deviation from ideal capacitive behavior. Sometimes calculated values of n slightly >1 where obtained for one of the CPEs. In those cases, there was little sensitivity of the fit to the choice of which element approached ideal behavior more closely. For those cases a value $n_2 = 1$ was imposed and n_F was allowed to vary; the resulting n_F was always >0.92 (subscripts are keyed to the element designations in Figure 7).

Figures 8 and 9 show as function of time examples of the nominal capacitance and polarization resistance results from the fitting procedures. Duplicate specimens showed similar trends. The value for C_F* was similar in both solutions (~3 to 10 $\mu F/cm^2$) and changed relatively little with exposure time. This result is consistent with the capacitance expected from a dielectric film of thickness L:

$$C_F^* = \frac{\varepsilon \cdot \varepsilon_0}{L} \qquad (2)$$

where ε_0 is the permittivity of vacuum and ε the dielectric constant of the film material, when for example L~5 nm and ε~9 (typical of naturally grown passive films on aluminum [15,16] and of solid or hydrated aluminum oxides respectively) are assumed which yields C_F*~1.60 $\mu F/cm^2$. Similar behavior on passive aluminum has been observed often [17] and supports the interpretation that the high frequency loop in the spectra corresponds to the passive film. The values for C_2^* in both solutions were larger (consistent with a pseudocapacitive origin) and showed more variability. In solution P, C_2^* showed strong momentary increases upon additions of extra $CaCO_3$.

The values of R_{P1} and R_{P2} for a given solution increased and decreased roughly together as exposure time progressed, in keeping with the assumption of coupling between their associated reactions responsible. In solution P the resistances decreased upon $CaCO_3$ addition matching coincident with the disturbances in C_2*, but later recovered and reached large values at 3,000 h. The polarization resistances in NP decreased substantially with time, reaching after 3,000 h values in the order of those encountered for solution C at similar exposure times.

In the following a working assumption is made that the high frequency limit resistance (R_{P1}) is approximately the same as that of a cathodic reaction under activation control, having a Tafel slope value β in the order of those of the intermediate reaction steps. Since the rate of the anodic reaction was considered to be nearly potential independent, a nominal corrosion current density can then be obtained as $i_{corr} \sim \beta / 2.3\ R_{P1}$. A value β ~ 160 mV was chosen, representative of those reported for likely reactions at an aluminum surface [(18)]). At long exposure times of ~3,000 h, R_{P1} is ~1.2 $10^7\ \Omega$-cm^2 and ~2 $10^5\ \Omega$-cm^2 for P and NP solutions respectively. The corresponding nominal corrosion rates are extremely small in the P solution (~60 nm/y) and higher but still modest (~3.5 μm/y) in the NP solution. These values are consistent with the visual observation of unblemished aluminized steel surfaces in both environments by the end of the exposure period. Thus, high total alkalinity regimes with or

without carbonate precipitating conditions do not appear to be adverse within the conditions and time exposure intervals examined. It is cautioned however that the rate estimated for the NP regime, if sustained, would mean penetration of the outer aluminized layer after a decade of service or so.

The EIS results for solution C were also simulated using the equivalent circuit in Figure 7. However, the meaning of the components in the lower branch is different than for solutions NP and P. In solution C there were macroscopic pits where active dissolution of aluminum was in progress, and the diagram conforms to previous representation of impedance of pitted aluminum [19]. The pits had likely nucleated around intermetallic precipitates and the long term increase in *If* impedance modulus may be associated with the progressive deactivation of pits after individual precipitate particles become isolated by localized corrosion products [20]. During the active period the pits were expected to be the locus of both cathodic and anodic reactions, with high local polarization admittance. The inverse of the integrated polarization admittance of all the active pits would then be represented by R_{P2}. Electrolytic current constriction around each pit [21] creates an ohmic resistance component, which upon parallel combination over all pits has an effect represented by R_{P1} (no longer of Faradaic origin as before). CPE_2 represents now the combined interfacial capacitance of the active pits, where directly exposed metal and tortuous geometry contribute to a greater specific capacitance than that of filmed passive aluminum.

The equivalent circuit fit calculations for solution C yielded suitable small values (~9 Ω to ~40 Ω, reported here as resistances not normalized for the ~95 cm^2 specimen area) for R_{P1}, consistent with an expected moderate localized solution resistance. Accordingly, R_{P2} was in the order of the *If* impedance modulus (~700 Ω early on, ~6 kΩ near the end of the test). Both capacitive elements had significant frequency dispersion: n_F ~0.57 to 0.66 (consistent with the highly distorted appearance of the high frequency loops in Figure 6) and n_2 ~0.68 to 0.80. The value of C_F* was small (~0.25 to ~1 μF/cm^2 surface-normalized value) and, considering the uncertainty inherent to the high frequency dispersion, consistent with the value obtained for the film capacitance in the other solutions. The values obtained for C_2* (~1.6×10^{-3} to 6.6×10^{-3} F, when non-surface normalized) appear however to be too high even allowing for frequency dispersion uncertainty, considering that they should approximately represent the total capacitance of a relatively small number of pits. This particular issue should be revisited in future research.

To estimate corrosion rates in the C solution tests, the same working assumptions were made as before but using only the value of R_{P2} and considering both anodic and cathodic reaction polarizability and thus obtaining a Stearn-Geary constant [22] half of that applied earlier. The result is surface-averaged corrosion rates ranging from ~12 μm/y early on to ~1.7 μm/y after ~3,000 h. Those values become important considering that the corrosion is strongly localized at least at the beginning, with consequent risk of aluminized layer penetration early in the life of a component exposed to similar media.

CONCLUSIONS

1. In >3,000h tests type 2 aluminized steel showed extremely low corrosion rates in an environment with some chloride but of high total alkalinity and calcium carbonate precipitating tendencies, supporting prior evidence in favor of a scale tendency criterion to predict corrosivity.

2. Corrosion performance was good over the test period in a high total alkalinity, but non-scale forming medium with some chloride. However, electrochemical impedance measurements indicate that some corrosion may be of importance over longer periods.

3. Exposure to the same chloride content but in the absence of alkalinity or precipitating hardness led to early pitting of the aluminized layer.

ACKNOWLEDGEMENTS

This investigation was supported by the Florida Department of Transportation and the Federal Highway Administration. The opinions and findings described here are those of the authors and not necessarily those of the funding agencies.

REFERENCES

1. H. Kimoto, Galvanic corrosion behavior of aluminized steel in seawater, Corrosion Engineering 48, p.579-588 (1999)

2. W.D. Cerlanek, R.G. Powers, Drainage Culvert Service Life Performance and Estimation, State of Florida Department of Transportation Report No. 93-4A, April 1993

3. G.E. Morris, L. Bednar, Comprehensive Evaluation of Aluminized Steel Type 2 Pipe Field Performance, G.E. Morris and L. Bednar, Published by AK Steel Corporation, Middletown, Ohio, 1998

4. L. Bednar, Galvanized Steel Drainage Pipe Durability Estimation with a Modified California Chart, Paper No. 88-0341, 68th Annual meeting, Transportation Research board, January 22-26, 1989, Washington, D.C., 1989

5. V.L Snoeyink, D. Jenkins, Water Chemistry, John Wiley & Sons, New York, 1980

6. F.C. Porter, S.E. Hadden, J. Appl. Chem., 3, p.385-409 (1953)

7. W. Li, S. Liu, Q. Huang, M. Gu, Coating structure and properties of continuously hot dipped aluminized steel wire, Materials Science and Technology, 19, p.1025-1028 (2003)

8. Metals Handbook, 8th Ed., Vol. 7, American Society for Metals, Ohio, 1972

9. P. Castro, A.A. Sagues, E.I. Moreno, L. Maldonado, J. Genesca, Characterization of activated titanium solid reference electrodes for corrosion testing of steel in concrete, Corrosion, 52, p.609-617 (1996)

10. K. Nisancioglu, Electrochemical behavior of aluminum-base intermetallics containing iron, J. Electrochem Soc. 137, p.69, (1990)

11. J.B. Bessone, D.R. Salinas, C.E. Mayer, M. Ebert, W.J. Lorenz, An EIS study of aluminum barrier-type oxide films formed in different media, Electrochimica Acta, 37, p.2283-2290, (1992)

12. J.H.W. de Wit, H.J.W. Lenderink, Electrochemical impedance spectroscopy as a tool to obtain mechanistic information on the passive behavior of aluminum, Electrochimica Acta, 41, p.1111-1119, (1996)

13. R.D. Armstrong, K. Edmondson, The impedance of metals in the passive and transpassive regions, Electrochimica Acta, 18, p.937-943, (1973)

14. I. Epelboin, M. Keddam, Faradaic Impedances: Diffusion impedance and reaction impedance, J. Electrochem. Soc., 117, p.1052-1056, (1970)

15. J. Bessone, C. Mayer, K. Juttner, W.J. Lorenz, Electrochimica Acta, 28, p.171, (1983)

16. Oxides and Oxide Films, Ed. J.W. Diggle, Vol. 1 Dekker, New York, 1972

17. Lee, W and Pyun, S: “Effects of hydroxide ion addition on anodic dissolution of pure aluminum in chloride ion-containing solution”, Electrochimica Acta, 44 (1999) 4041-4049.

18. R.D. Armstrong, V.J. Braham, Corrosion Sci., 38, p.1463-1471, 1996

19. H. Shih, F. Mansfeld, Corrosion, 45, p.610, 1989

20. R. Gundensen, K. Nisancioglu, Corrosion, 46, p.279, 1990

21. R. Oltra and M. Keddam, Corrosion Sci. Vol.28, p.1 (1988)

22. D. A. Jones, Principles and prevention of Corrosion, 2nd Ed. Prentice Hall, Upper Saddle River, 1996.

TABLE 1
Chemical composition of steel substrate (% weight)

C	Mn	P	S	Si	Cu	Al	Cb	Ni	Cr	Ti	N	Mo	Fe
0.05	0.20	0.006	0.012	0.01	0.031	0.041	0.002	0.017	0.028	0.002	0.0036	0.003	Bal.

Mill test report provided by Contech Construction Products Inc.

TABLE 2
Synthetic solutions composition and target properties

Solution	TA mg/L $CaCO_3$	TH mg/L $CaCO_3$	FC mg/L	BI	$[Ca^{+2}]$ mg/L	σ μS/cm
C (control)	0.05	0	0	0.05	0	1330
NP (non precipitating)	491	0	23	468	0	2240
P (precipitating)	491	499	23	967	200	2340

Legend: TA=total alkalinity, TH=total hardness, FC=free CO_2, BI=Bednar Index, σ=conductivity
pH = 7.5
$[Cl^-]$ = 372 mg/L

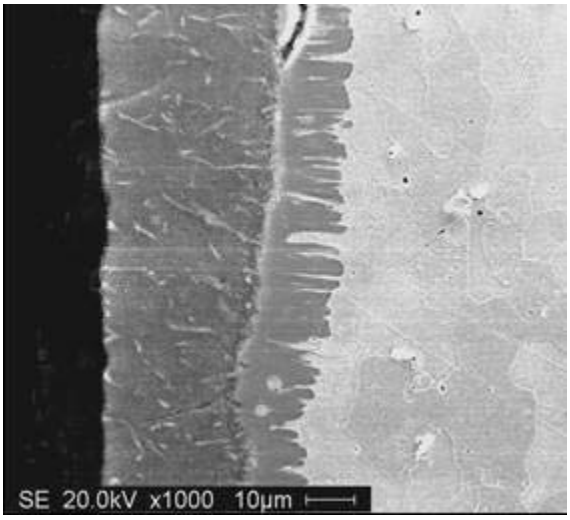

FIGURE 1 - Cross section of a 1.59 mm thickness flat T2AS specimen after etching with 2% Nital solution

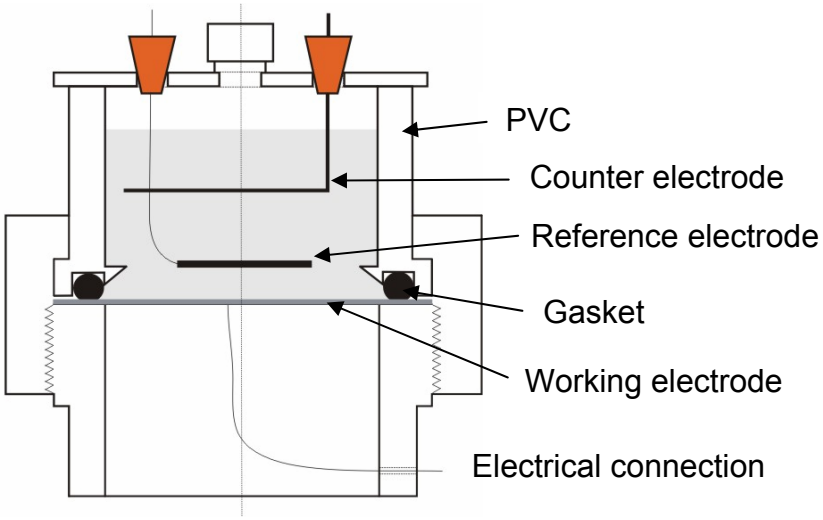

FIGURE 2 - Test cell arrangement

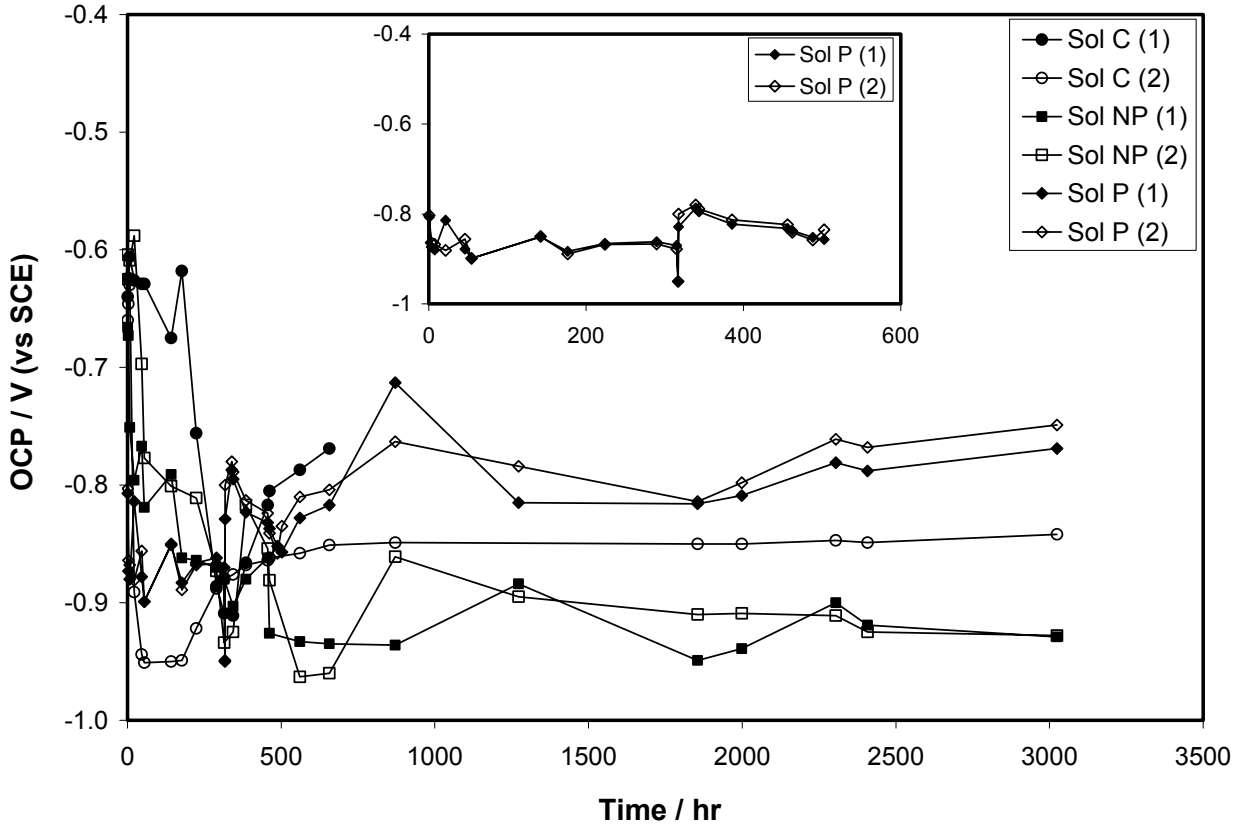

FIGURE 3 - OCP evolution as a function of exposure time

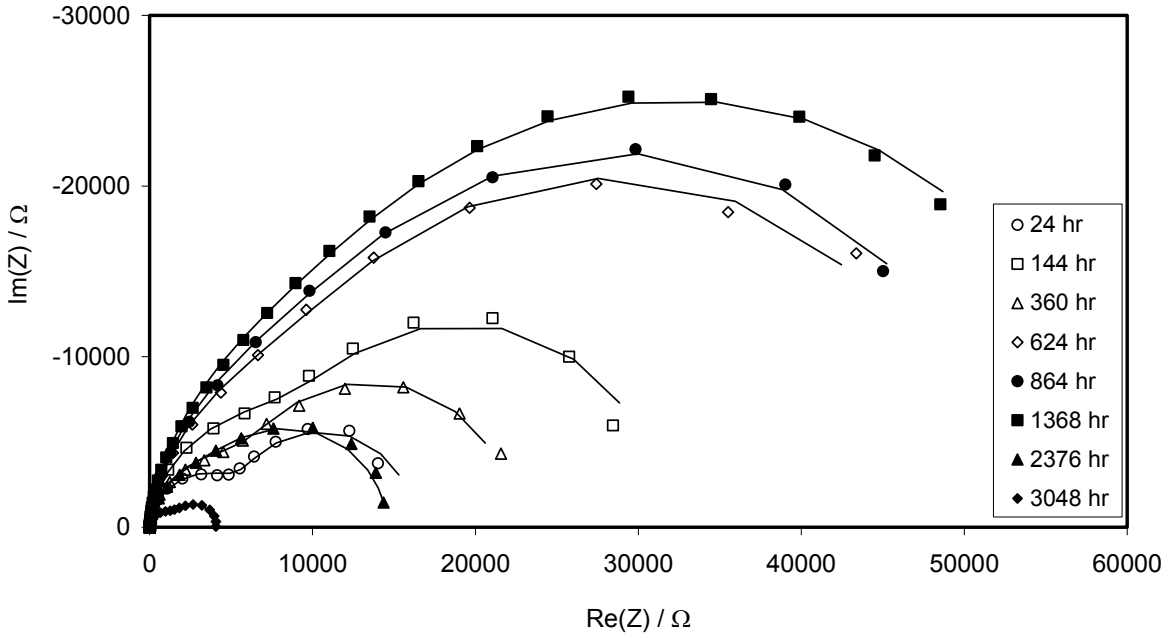

FIGURE 4 - OCP EIS behavior in solution NP (300 kHz – 1 mHz, 5 points/decade). Area = 95 cm^2

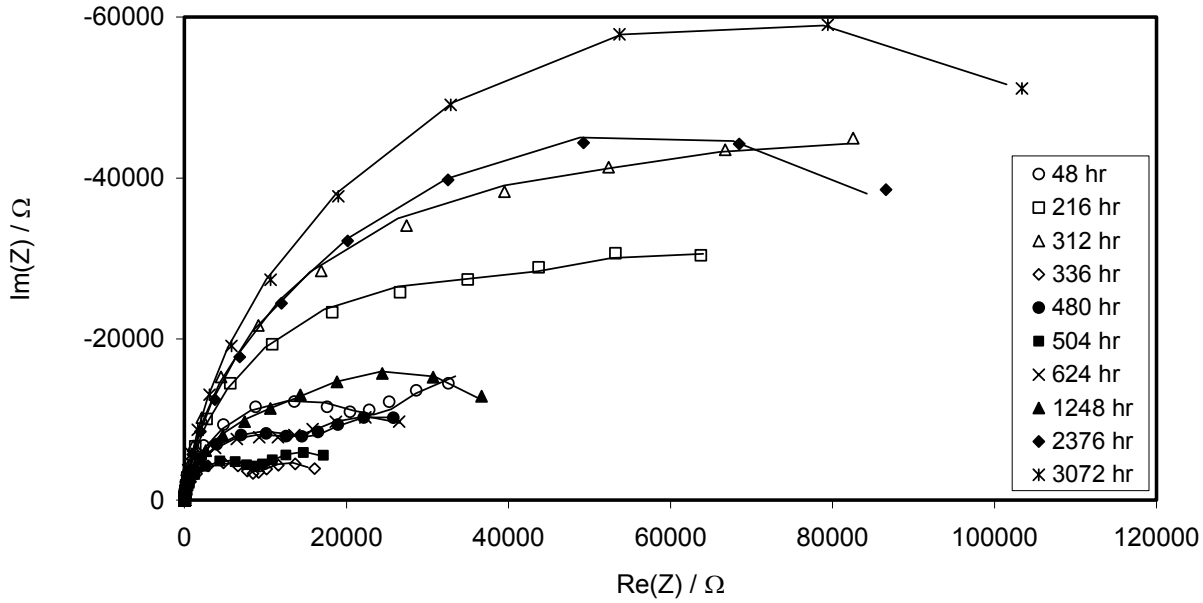

FIGURE 5 - EIS behavior in solution P (300 kHz – 1 mHz, 5 points/decade). Area = 95 cm^2

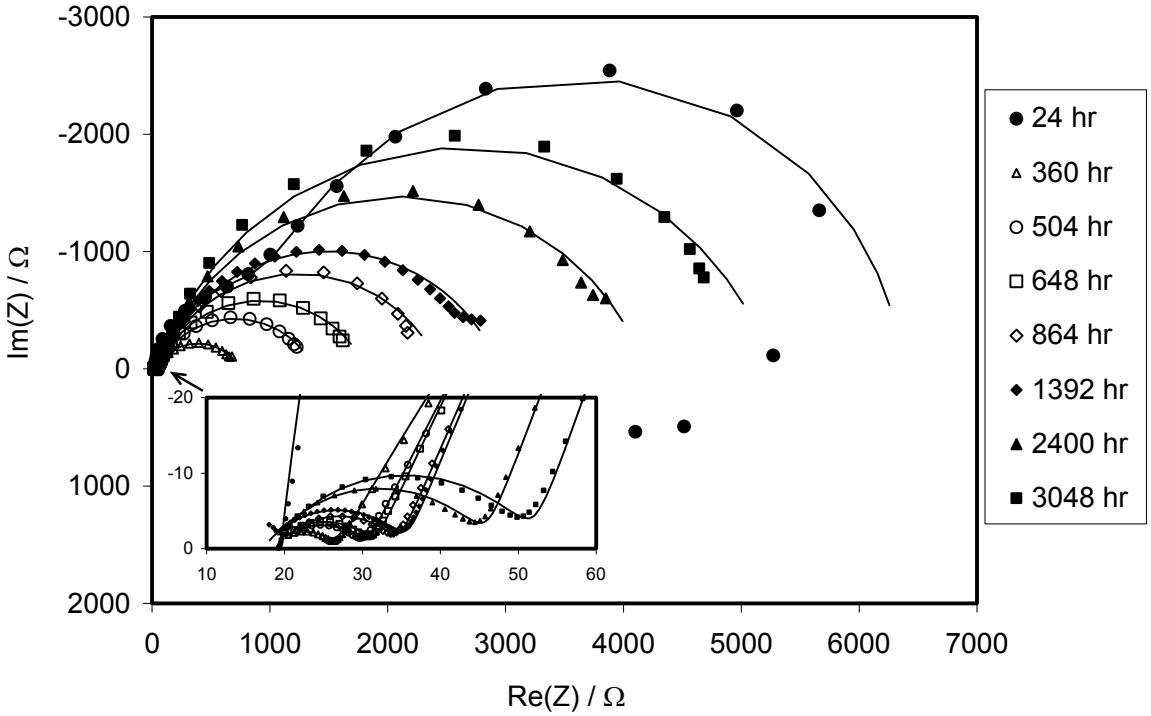

FIGURE 6 - EIS behavior in solution C (300 kHz – 1 mHz, 5 points/decade). Area = 95 cm^2

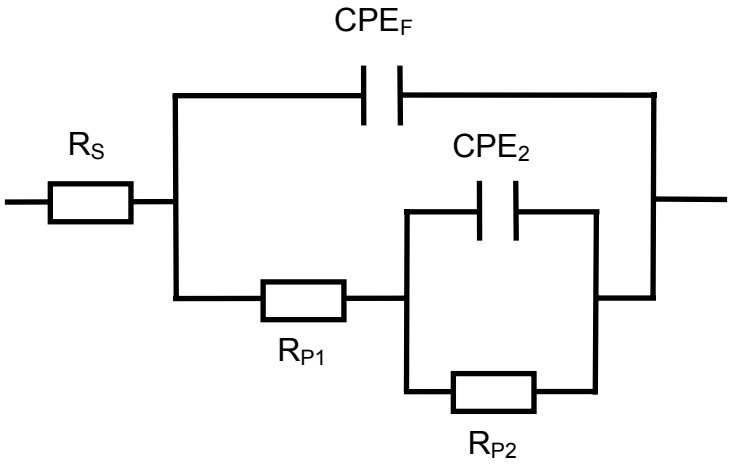

FIGURE 7 - Equivalent circuit to simulate the EIS response

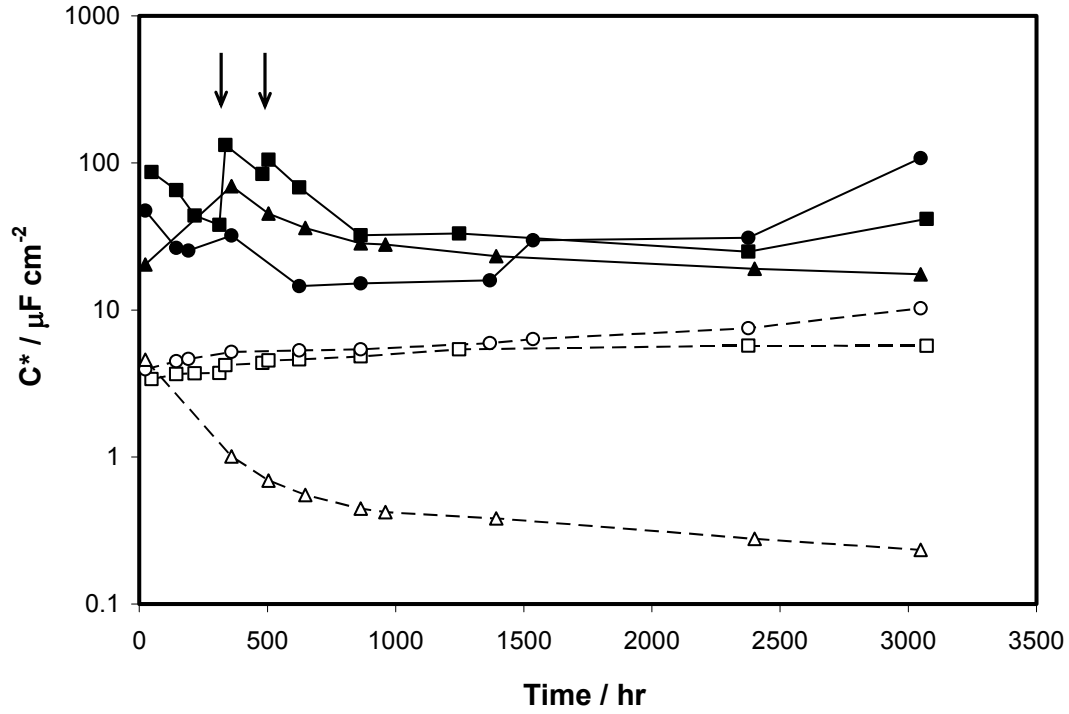

FIGURE 8 - Evolution of the nominal capacitance C* as a function of time in solutions NP (circles), P (squares), and C (triangles) (---C_F*, ─ for C_2*). Arrows indicate $CaCO_3$ additions in solution P.

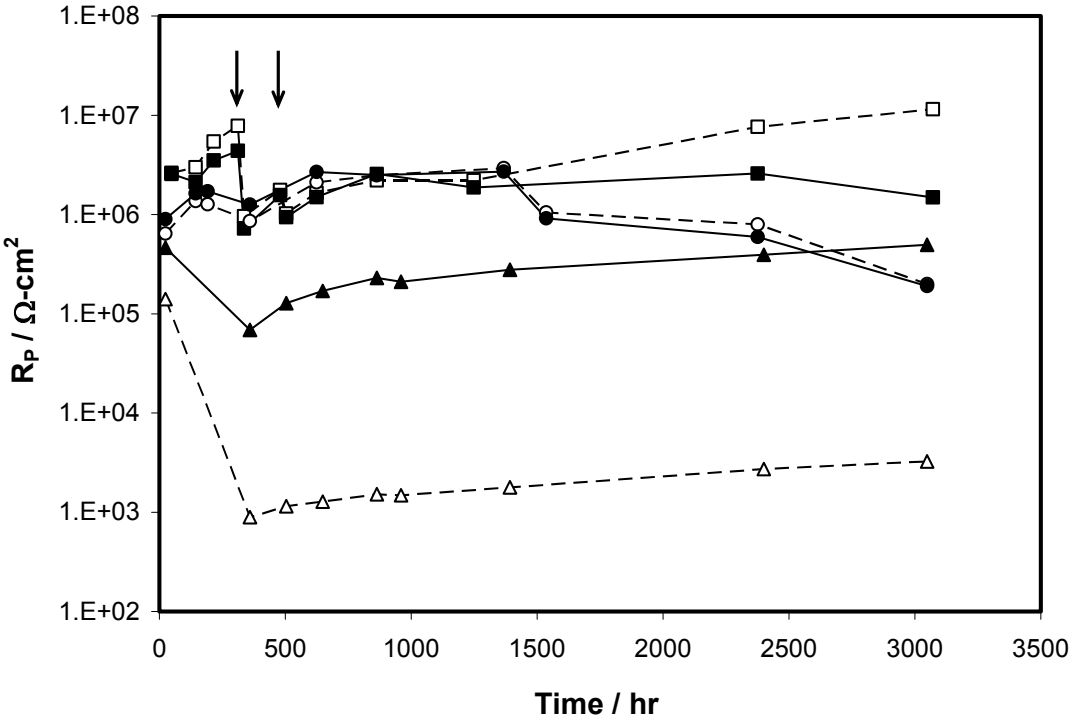

FIGURE 9 - Evolution of the polarization resistance components as a function of time in solutions NP (circles), P (squares), and C (triangles) (--- R_{P1}, ─ R_{P2}). Arrows indicate $CaCO_3$ additions in solution P.